Spectral Classification and Cloning of Photonic Integrated Filters for Volume Testing

Matteo Petrini, Moritz Seyfried, Francesco Morichetti and Andrea Melloni

***Abstract*— Volume testing is rapidly becoming a key step in the production chain of photonic integrated circuits (PICs), which are ever increasing their integration density and complexity, and are penetrating many market sectors. What makes PIC testing peculiar with respect to testing of electronic integrated circuits (EICs) is that it generally requires also control and calibration procedures. Here, we present a method to perform time and cost-efficient volume testing of frequency-selective PICs. The described techniques enable to evaluate the deviation between the spectral response of a device under test (DUT) and a reference (REF) device, without a direct measurement of the DUT spectral response, which is a time and resource consuming procedure. Information on the DUT status is inferred from the integral power of a top-flat broadband optical source, which is shaped by the REF device and is transmitted thought the DUT. In this way it possible to classify the DUT according to specifically defined metrics, automatically tune the DUT to replicate the REF spectral response and build LookUp Tables (LUTs) to be used in operative conditions. The proposed technique is validated experimentally on a reconfigurable silicon-photonics microring resonator filter implementing a Tuneable Optical Add/Drop Multiplexer, but we also provide conditions for its use for testing of frequency-selective devices.**

***Index Terms*— Integrated photonics, classification, volume testing, control, calibration, microring resonators, optical filters.**

I. Introduction

THE term "testing" identifies a class of operations to be performed during the production chain of any device, system, software or whatever. It is a very demanding process, typically requiring large time and cost efforts to extract the required information. In many fields, such as in electronic integrated circuits (EICs) and MEMS, testing is a real discipline and it is becoming of vital importance also in photonics, where photonic integrated circuits (PICs) are penetrating many market sectors and are increasing their integration density and complexity [1].

Testing of integrated circuits includes the assessment of the technological process, the quality of the various building blocks, the entire device functionality and even the "product", including control and driving electronics and software. It can be interpreted as qualification, verification, validation, and characterization [2]. If for a simple device the measurement of a few significant parameters could suffice, for reconfigurable, programmable and in general complex circuits, testing cannot be separated from a calibration, tuning or programming process that becomes an essential part of the testing itself. For these reasons, tools and techniques for functional testing of PICs (possibly at wafer level but not limited to this scenario) are getting urgent [3] [4]. With respect to EIC testing, PIC testing has some peculiar aspects: i) many devices integrated in photonic chips, such as photodetectors, thermal tuners or p-n junctions, require both electrical and optical signals to be processed (often simultaneously); ii) for many applications either the time and/or frequency domain functionality has to be evaluated and classified [5]; iii) due to fabrication imperfections, assessment of PIC behavior could be impossible in "as-built" devices [6] [7] [8]; therefore, testing is not only a synonym of "measurement" but involves also control and calibration procedures.

Control and calibration procedures are usually implemented by means of feedback-controlled systems [9] [10], composed by sensors, actuators and electronic drivers. Sensing can be performed either on the light coming from the output ports of the device, using integrated or external photodetectors [11], or directly inside the chip [12] [13]. Actuation instead mainly relies on thermo-optic [14] or electro-optic effect [15]. Regardless the exploited effect, actuators are driven by suitable control boards, such as microprocessors, Field Programmable Gated Arrays (FPGAs), microcontrollers or custom electronics [16]. Based on the information provided by sensors, control algorithms, such as like homodyne locking [17], dithering [18] or optimization (i.e., maximum/minimum search) [19], are executed to steer and hold the PIC in the desired working point.

For frequency selective devices, typical calibration metrics rely on the minimization of the Mean Squared Error (MSE) between the spectral response of the device under test (DUT) and a target spectral mask. An example is shown in the scheme of Fig. 1(a), where the spectral response of the DUT is measured by using a Tuneable Laser Source (TLS)

Matteo Petrini, Francesco Morichetti and Andrea Melloni are with the Department of Electronics, Information and Bioengineering (DEIB), Politecnico di Milano, 20133 Milano, Italy (email: matteo.petrini@polimi.it; francesco.morichetti@polimi.it; andrea.melloni@polimi.it). Moritz Seyfried is with Ficontec Service GmbH, Rehland 8, 28832 Achim, Germany (email: moritz.seyfried@ficontec.com).

M. P., F. M. and A. M. are co-inventors of a patent owned by Politecnico di Milano in the technical field of the publication.

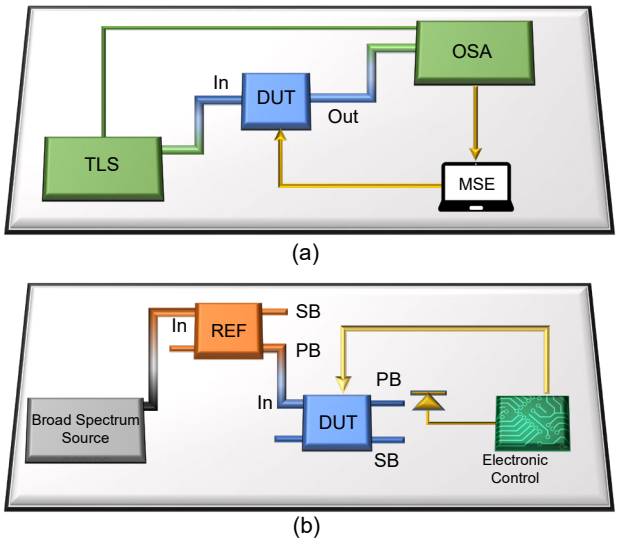

Fig. 1. (a) Conventional scheme to assess the quality of a device under test (DUT). A Tunable Laser Source (TLS) synchronized with an Optical Spectrum Analyzer (OSA) measures the DUT spectral transfer function. A computer estimates the deviation from the reference spectral response. (b) Proposed scheme: a broadband source feeds the reference device REF cascaded to the DUT, having passband PB and stopband SB ports. The integral output power is used by an electronic controller to estimate the spectral deviations between REF and DUT. Both schemes can provide a feedback signal to calibrate the DUT.

synchronized with an Optical Spectrum Analyzer (OSA). The deviation with respect to the desired response is calculated by a computational unit, which provides the feedback control signals to adjust the PIC actuators. Although simple and effective, the acquisition of the DUT spectral response and the MSE computation are typically time and resource consuming, this being not compliant with requirements of volume testing.

In this work we introduce and validate a fast and effective method of testing enabling to: i) compute the deviations between a DUT and a desired reference (REF) device, without measuring the spectral response; ii) classify the DUT according to specific metrics; iii) automatically tune the DUT to match the REF spectral response; iv) store the control parameters of the DUT in a Look-Up-Table (LUT) to be used for control and calibration in operative conditions. As shown in the block scheme of Fig. 1(b), the main idea of the proposed method relies on the use of a top-flat broadband optical source, which is shaped in the frequency domain by the REF device and is coupled to the DUT. The REF device can be integrated in the same chip of the DUT, but more generally an external device can be used. Our results show that, for a wide class of frequency-selective devices, the integral optical power at the DUT output provides direct information on its status and it can be also used to make its spectral response be a "clone" of the REF spectral response. The proposed technique is mathematically explained in Section II and numerically validated through numerical simulations in Section III. In Section IV we experimentally prove the approach, which is applied to a complex PIC, i.e., a 4-channel hitless Tuneable Add/Drop Multiplexer, operating in Dense Wavelength

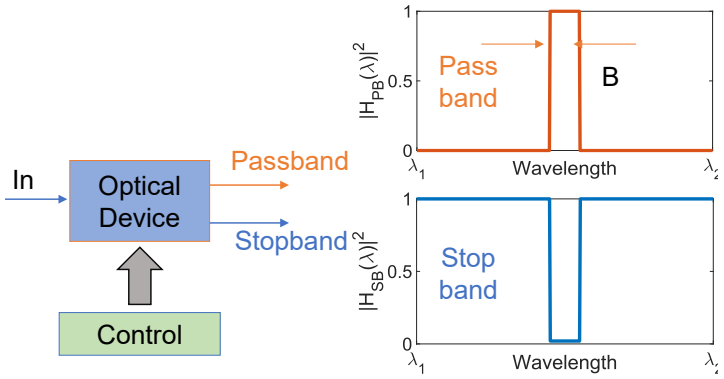

Fig. 2. (a) Scheme of a tunable optical device with two complementary output ports, stopband and passband. In-Passband and In-Stopband frequency response.

Division Multiplexing (DWDM) context.

II. The Cloning Technique

The proposed technique is based on the scheme of Fig. 1(b). A broadband spectral source, with a constant Power Spectral Density (PSD) S_0 across the operative wavelength range of the device, is coupled to the input port of the REF device. The DUT is cascaded to the REF device and a photodetector is connected at its output port.

In this work we consider wavelength-selective devices with a bandpass (PB) and/or a stopband (SB) spectral response $H_{PB}(\lambda)$ and $H_{SB}(\lambda)$, respectively, but the approach is valid even for multiport devices. The device has a bandwidth B and operates in the wavelength range between λ_1 and λ_2. We also assume that the spectral transfer function can be adjusted by using suitable integrated actuators. Typical wavelength selective filters have a flat-top response with a high rejection both in-band and out of band, that is $|\overline{H_{PB}}(\lambda)|^2 >> |\overline{H_{SB}}(\lambda)|^2$ within B and $|\overline{H_{PB}}(\lambda)|^2 << |\overline{H_{SB}}(\lambda)|^2$ otherwise, where $\overline{H_{PB}}(\lambda)$ and $\overline{H_{SB}}(\lambda)$ are the nominal spectral responses. This situation is

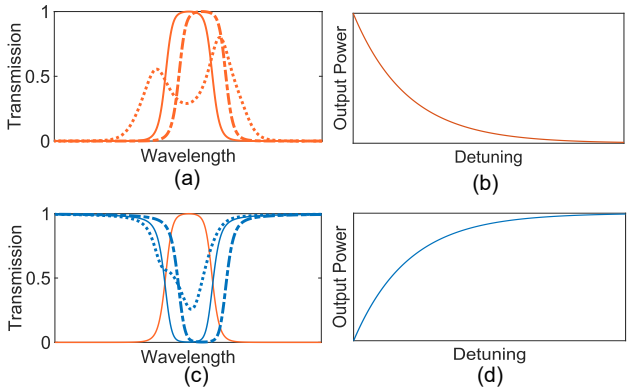

Fig. 3. (a) Typical passband REF device (solid line) and detuned (dotted) and shifted (dash-dotted) DUT spectral responses. (b) Dependence of the output power P_{OPP} vs detuning or shifting. The output power P_{OPP} is maximum for two identical devices and decreases with their spectral difference. (c) and (d) same for passband-stopband combination. The output power P_{OPS} is minimum when the REF and DUT match.

sketched in Fig. 2 showing the ideal passband $|\overline{H_{PB}}(\lambda)|^2 = 1$ and stopband $|\overline{H_{SB}}(\lambda)|^2 \approx 0$ responses within B for a lossless device.

If the passband output of both REF and DUT are used [as in the case shown in Fig. 1(b)], the PSD $S_{P,REF}(\lambda)$ at the output of the REF device,

$$S_{P,REF}(\lambda) = S_0\,|\overline{H_{PB}}(\lambda)|^2, \qquad (1)$$

is used as source for the DUT, so that the PSD $S_{P,\,DUT}(\lambda)$ at the passband port of the DUT, is

$$S_{P,DUT}(\lambda) = S_0|\overline{H_{PB}}(\lambda)|^2\left|H_{PB,DUT}(\lambda)\right|^2. \qquad (2)$$

When the DUT is tuned to its nominal state, $H_{PB,DUT}(\lambda) = \overline{H_{PB}}(\lambda)$, the integral power P_{OPP} measured by the detector is

$$P_{O_{PP}} = \int_{\lambda_1}^{\lambda_2} S_{P,DUT}(\lambda)\,d\lambda = \\ = S_0 \int_{\lambda_1}^{\lambda_2} |\overline{H_{PB}}(\lambda)|^4\,d\lambda \approx S_0\,B, \qquad (3)$$

where the losses are not accounted (just acting as a scaling factor), and the approximation is valid for a flat-top passband spectral response as the one in Fig. 2. In this case the output power P_{OPP} is the maximum achievable and the DUT is a clone of the REF device. If the DUT is not properly tuned, the in-band response is distorted without a flat top characteristic and the total output power is lower. In some cases [20], the filter bandwidth can be narrower than the desired nominal value and also in this case P_{OPP} is lower. It should be noted that, if the DUT is a tuneable-bandwidth device, its maximum bandwidth has to be narrower than or equal to the bandwidth of the REF. In fact, if the DUT could assume a bandwidth larger than that of the REF device, the output power maximization procedure described in eq. (3) could lead to over-sized bandwidth of the DUT with respect to REF.

The same behavior occurs even in case of a perfectly tuned DUT characteristic but spectrally shifted with respect the REF device by Δf. In this case P_{OPP} decreases by $\Delta P_{OPP} = S_0\,\Delta f$ with respect to the maximum $P_{OPP}=S_0B$ and vanishes when $\Delta f=B$; in other words, the relative output power variation depends on the spectral shift of the two devices as $\Delta P_{OPP}/P_{OPP} = \Delta f/B$. Therefore, the integral output power is a metric of the similarity of the REF and DUT devices, and its maximization provide a suitable criterion to drive the tuning of the DUT response $H_{PB,DUT}(\lambda)$ and clone the REF behavior $\overline{H_{PB}}(\lambda)$.

Similarly, the stopband port SB can be used for both REF and DUT and also in this case the maximization of the output power guarantees the proper spectral cloning of the two devices. In practice, since the devices comparison is related to their out of band behavior, the result is usually not as accurate as the maximization of the passband response.

The cascade of a passband and a stopband characteristic (or viceversa) can be also used, but it requires the minimization of the output power, given by

$$P_{OPS} = S_0 \int_{\lambda_1}^{\lambda_2} |\overline{H_{PB}}|^2 |H_{SB,DUT}(\lambda)|^2\,d\lambda \\ = S_0 \int_{\lambda_1}^{\lambda_2} |\overline{H_{PB}}|^2 (1 - |H_{PB,DUT}(\lambda)|^2)\,d\lambda \\ \approx S_0\big(B - (B - \Delta f)\big) = S_0\Delta f \qquad (4)$$

where the approximation is valid for a flat top spectral response shifted by Δf with respect the nominal REF device. The absolute output power variation is $P_{OPS} = S_0\Delta f$, and P_{OPS} vanishes for a perfectly cloned DUT (again losses are just a scaling factor).

The combinations REF(passband)-DUT(passband) and REF(passband)-DUT(stopband) are shown in Fig. 3(a)-(c), respectively. A qualitative dependence of the output power vs detuning and spectral alignment of the DUT, for the two scenarios, are shown in Fig. 3(b)-(d). In general, the combination of the two complementary behaviors shows a better sensitivity to the DUT tuning, especially for low selectivity devices, with the minor disadvantage to operate with weak output power levels.

A common metric to evaluate the difference between two

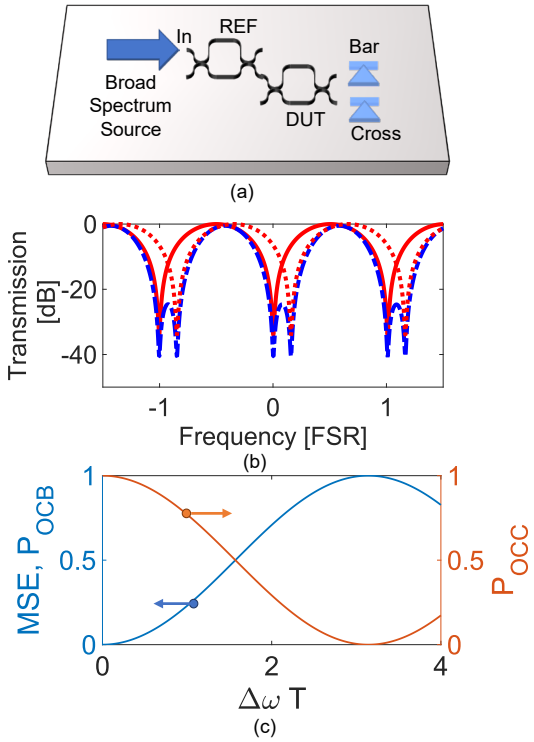

Fig. 4. (a) Cascade of the MZI-REF and MZI-DUT for testing and calibration. (b) Spectral responses of REF (solid red line), DUT shifted by Δω (dashed red line) and their product (in dashed blue line). (c) Dependence of MSE and P_O vs Δω. Normalized P_O depends on MZI connection. P_{OCB} in case of REF(cross)-DUT(bar) (or viceversa) and P_{OCC} in case of REF(cross)-DUT(cross).

devices is the Mean Squared Error (MSE) between their spectral responses

$$MSE_x = \frac{1}{N}\sum_{i}^{N}(|H_{x,DUT}(\lambda_i)|^2 - |H_{x,REF}(\lambda_i)|^2)^2 \qquad (5)$$

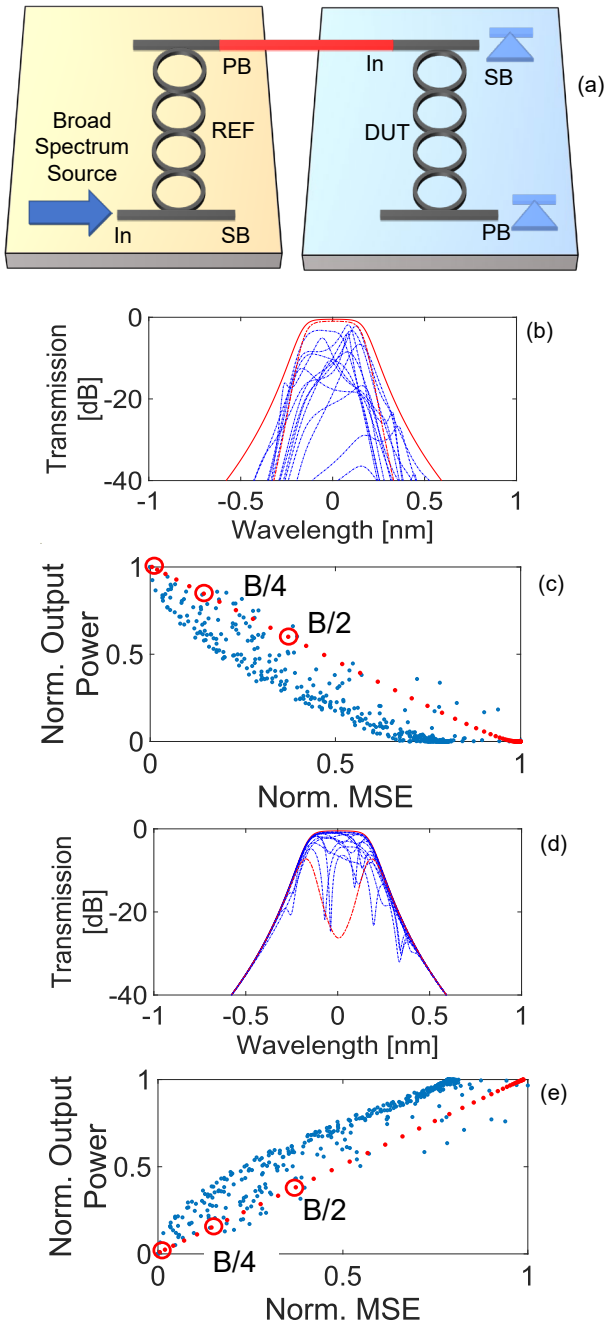

Fig. 5. (a) Schematic of the testing system for 4 cascaded-MRR filter. REF is external with respect to the DUT and their optical connection is highlighted in red. (b) Squared modulus of REF spectral response passband (solid red plot), spectral response of the cascade REF-passband DUT optimally tuned (dashed red plot) and spectral response of the cascade REF-perturbed passband DUT (dashed blue plots). (c) MSE (normalized to worst case, i.e., when all the rings have a phase shift of π) vs. integral output power (collected at the output of the series passband-passband). Its maximum is when REF and DUT match. Red points represent the case of DUT nominal tuning but rigidly shifted in frequency. Points related to a detuning of B/4 and B/2 are highlighted. (d) same of (b), considering DUT stopband port. (e) Normalized MSE vs. integral output power (collected at the output of the series passband-stopband). Its minimum is when REF and DUT match. For sake of visualization not all the simulated cases are shown in (b) and (d).

where N is the number of the acquired sampled wavelengths λ_i and x is referred to passband (PB) or stopband (SB). It is convenient to define the total MSE as the summation of the two,

$$MSE = MSE_{SB} + MSE_{PB}. \quad (6)$$

In the next sections it is demonstrated that the MSE between spectral responses of two frequency-selective devices is strongly correlated with the output power P_{OPP} or P_{OPS} defined above. Hence this quantity is a good estimator of the MSE and it can be used as significative value for testing, classification and calibration aims or as a feedback signal for real time control purposes.

III. Numerical Results on Test Structures

In this section we show numerically that the optical power $P_{O_{PP}}$ and $P_{O_{PS}}$ defined in Eqs. (3) and (4) are a good estimator of the MSE between the spectral response of the DUT and that of the REF and can guide the tuning of the DUT to clone the spectral response of the REF.

To this aim, we start considering the case of Fig. 4(a) where the REF and DUT devices are ideal Mach-Zehnder Interferometers (MZIs) with 50:50 directional couplers. The transfer function is $|H_{MZ,C}(\omega)|^2 = \cos^2(\omega T/2)$ at cross port and $|H_{MZ,B}(\omega)|^2 = \sin^2(\omega T/2)$ at bar port, being ω the angular frequency and T the unbalance in time unit. If the spectral width of the broadband source is larger than the Free Spectral Range (FSR) of the MZI, the integral output power (generically labeled as P_O) from the cascade of the two devices misaligned by Δω [the spectral responses are shown in Fig. 4(b)], can be analytically calculated and is proportional to $P_O \propto 2\pm\cos(\Delta\omega T)$. The ± sign depends if the two MZI are connected on the same port (bar-bar or cross-cross) or crossed. In this case, the MSE can be analytically computed as MSE = -cos($\Delta\omega T$). Figure 4(c) shows the MSE and the normalized P_O versus $\Delta\omega T$. The output power referred to the cascade REF (cross)-DUT (bar) (and viceversa) is labelled as P_{OCB}, while P_{OCC} is the power referred to the cascade REF (cross)-DUT (cross). These curves indicate that the optical power P_O provides direct information for the evaluation and minimization of the MSE. Note that the absolute value of the output power does not affect the results.

Similar results are obtained with other simple circuits such as microring ring resonators (MRR), Fabry-Pérot cavities or Bragg gratings, that being highly spectrally selective, can show a P_O strongly dependent on the detuning, with a very large difference between maximum and minimum.

As an example of complex PIC, we consider the 4-MRR filter of Fig. 5(a). The device has a bandwidth B = 40 GHz, MRR radius 10 μm and group index n_g =3.89 (FSR=1.2 THz), with power coupling ratios equal to [0.282, 0.0099, 0.0035, 0.0085, 0.236]. These coupling ratios provide an optimized Chebyshev response and are slightly asymmetric as round-trip losses, 0.1 dB/turn, are considered. The Drop port (passband) of the REF device is connected to the DUT filter and the output power can be acquired at the Drop port, P_{OPP}, or at the Through port, P_{OPS}. The nominal spectral characteristic at the Drop port $|\overline{H_{PB}}(\lambda)|^2$ is reported in Fig. 5(b) (red solid line) and the REF-DUT cascade in nominal condition, $|\overline{H_{PB}}(\lambda)|^4$, in red dashed line.

To consider a realistic case, uncorrelated phase perturbations uniformly distributed in the interval ± π are applied to each MRR of the filter, while the coupling elements are assumed equal to the nominal values. The spectral responses at the Drop output of the DUT, $\overline{|H_{PB}(\lambda)|^2}$ $|H_{PB,DUT}(\lambda)|^2$, are reported as blue dashed line in Fig. 5(b). For each considered phase perturbed DUT, the total MSE = MSE_{PB} + MSE_{SB} is calculated, as well as the output power P_{OPP}, assuming an input PSD S_0 broader than B. P_{OPP} and the correspondent MSE (normalized to its maximum, i.e., when all the rings' perturbations are equal to π) are reported in Fig. 5(c). Their strong correlation is evident, and the integral output power is maximum when MSE vanishes and decreases accordingly. Analogously, the PSD at the Through port of the DUT and the MSE-P_{OPS} correlation are shown in Fig. 5(d)-(e).

In Figs. 5(c) and (e) the red lines represent, respectively, the MSE-P_{OPP} and MSE-P_{OPS} in case of a DUT nominally tuned but shifted by Δf with respect to the REF device; as discussed in Sec. II, P_{OPP} (P_{OPS}) decreases (increases) almost linearly with Δf, vanishing when Δf is comparable to B (when Δf=0). In both cases the integral output power is a reliable indicator of the quality of the DUT tuning. This means that, by setting a threshold on P_{OPP} or P_{OPS} in the testing procedure, it is possible to select the DUT that can be classified and considered acceptable or unsuitable according to the required specifications, without the need for measuring neither the MSE nor the spectral response. More conveniently, during testing procedures the relative power P_{OPP}/P_{OPS} can be evaluated in order to remove uncertainties in the absolute power, which can originate from tolerances in the coupling efficiency at the optical I/O ports.

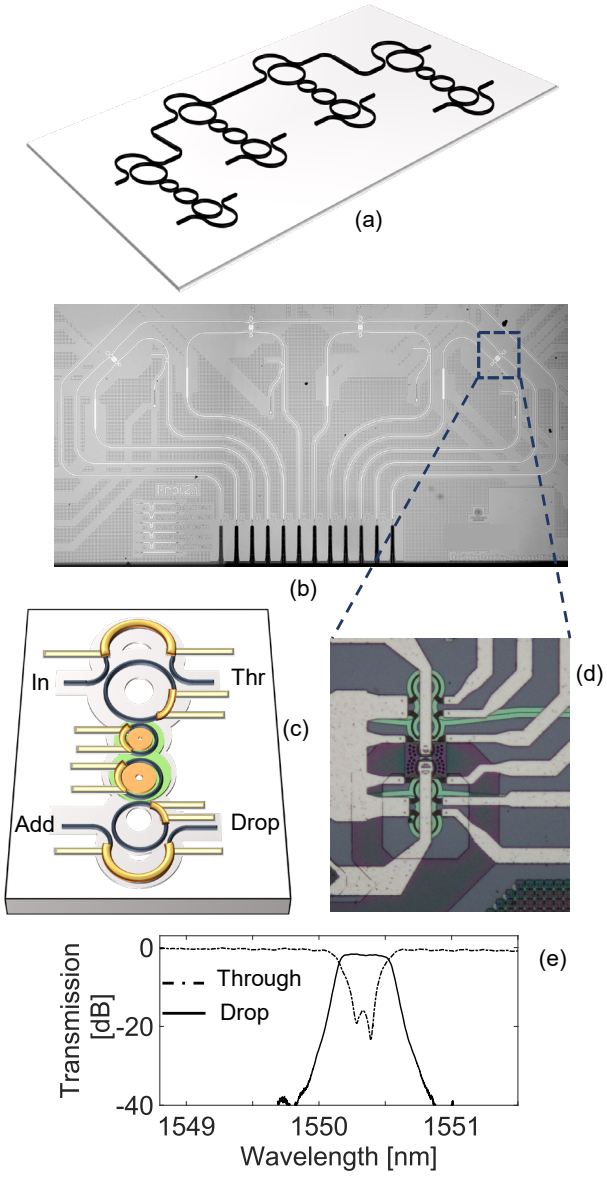

Fig. 6. (a) Block scheme of the employed Tuneable Optical Add-Drop Multiplexer (TOADM) and (b) its microphotograph. (c) Schematic topology of MRR based filter, constituting the single channel of the TOADM. (d) Filter microphotograph, where heaters and p-i-n junction for hitless operation can be recognized. (e) Spectral response (Through and Drop port) of the single REF filter.

IV. Experimental Results: Filter Cloning

In this section we provide experimental evidence of the effectiveness of the proposed method by demonstrating the automatic testing and calibration of a 4-channel Tunable Optical Add Drop Multiplexer (TOADM) in silicon photonics. The TOADM has been fabricated on a commercial Silicon-On-Insulator (SOI) platform (Advanced Micro-Foundry, AMF) [21]. The block scheme of the TOADM is shown in Fig. 6(a), together with a top-view chip photograph in Fig. 6(b); the scheme and photo of a single filter of the TOADM architecture are shown in Figs. 6(c) and (d), respectively. All the details on the filter design and technology can be found in [22]. To summarize here the main features, each filter consists of four coupled MRRs with MZI-based tunable couplers to control the coupling with the input/output bus waveguides. Each MRR has a thermo-optic actuator for wavelength tuning and the two central MRRs are equipped with p-i-n junction attenuators for hitless operation [22]. A Vernier scheme with MRR diameters of [29.2 16.8 20.4 24.4] μm is adopted to obtain an FSR-free spectral response that can be hitlessly tuned across a wavelength range wider than 100 nm. The measured frequency response of the reference filter (in case of nominal tuning) is reported in Fig. 6(e). The Drop-port 3dB-bandwidth is about 40 GHz and the isolation, evaluated at 50 GHz from the center of the passband, is more than 30 dB, while the Through port in-band-rejection is around 18 dB, averaged on 20 GHz around the central frequency.

According to the method described in Sec. II, to perform the testing and tuning of the spectral response, we used as broadband source the Amplified Spontaneous Emission (ASE) noise from an Erbium Doped Fiber Amplifier (EDFA), but a super luminescent diode or other broadband sources could be used as well. The only requirement is that the spectrum of the source has to be larger than the operation wavelength range of the filter. The PSD at the Drop port of the REF filter serves as input of the TOADM under test. The REF filter, nominally identical to those of the TOADM, has been previously tuned exploiting the conventional approach of Fig. 1(a), to the desired

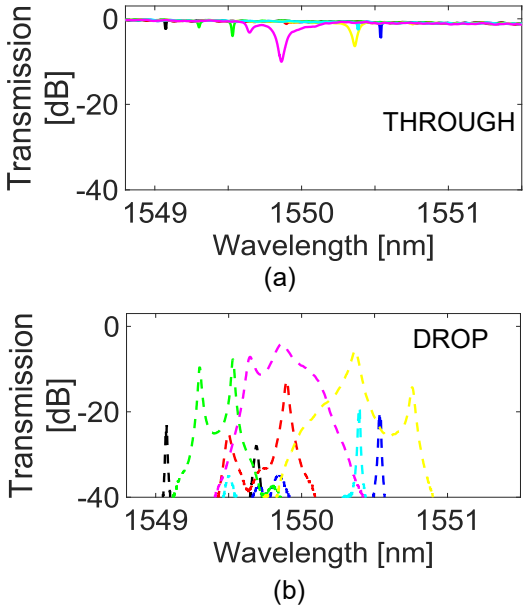

Fig. 7. As built frequency response of eight different DUTs at Through (a) and Drop (b) ports. Two different TOADM chips are considered.

transfer function shown in Fig. 6(e). This is basically the PSD used to test the TOADM.

The filters of the TOADM can be conveniently disconnected from the bus by means of the central rings' attenuators and the tunable MZ couplers. This enables sequential testing and tuning the different filters of the TOADM, because only one filter at a time can be connected and tested, while the other three filters are kept disconnected. At the initial stage, the spectral responses of all the as-fabricated filters under test have a random behavior because of the spread of the MRR resonances due to fabrication imperfections. In Fig. 7(a) and 7(b) the different initial condition of eight filters belonging to two different TOADM chips are shown.

The electronic control unit of the testing system uses an external photodetector and drives the thermo-optic actuators of the DUT according to a steepest descent gradient algorithm and dithering signals [23] [24]. The control strategy that we used consists of two steps: i) the optical power P_{OPP} at the Drop port of the DUT is acquired and maximized. This enable a coarse but fast tuning even if the initial condition of the spectral response is far from being similar to the target; ii) the P_{OPS} from the output Through port of the TOADM is minimized, achieving a very precise tuning of the spectral response.

Figures 8(a) and 8(b) show the tuned spectral responses for the eight considered filters, respectively at Through and Drop ports. Spectra have been collected choosing a wavelength span of 2.6 nm, with a wavelength sampling of 1 pm. The orange solid curve represents the spectral response of the reference device. Results show an excellent overlap of the achieved tuned spectral responses for all the considered devices. The voltages applied to the thermal actuators need to be as accurate as 1 mV and weighted by specific coefficients to cancel unwanted thermal crosstalk effects [25]. Control signals are progressively adapted in order to optimize speed and accuracy of the

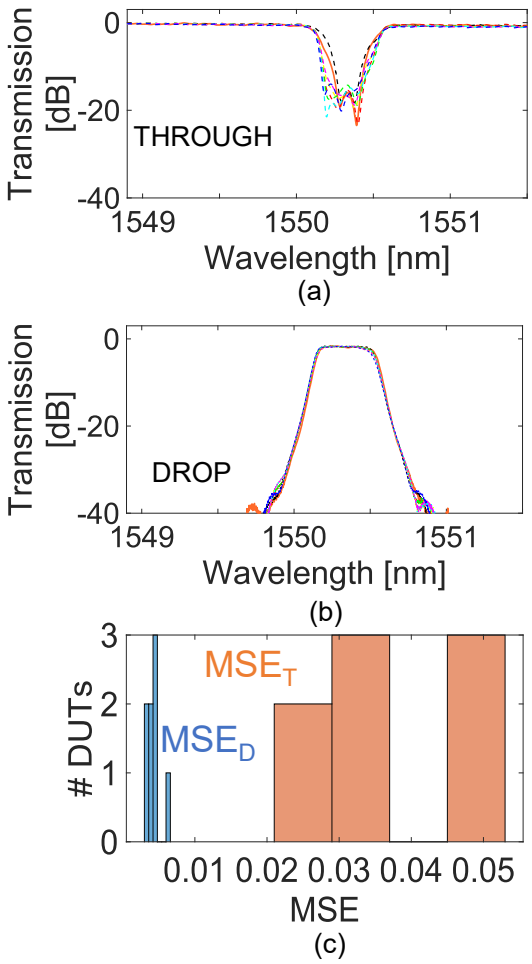

Fig. 8. Frequency response of the 4th order hitless MRR filter cloned with the described technique for both Through (a) and Drop (b) ports. (c) Histogram of the computed MSE between the reference and each tuned DUT for both Drop and Through.

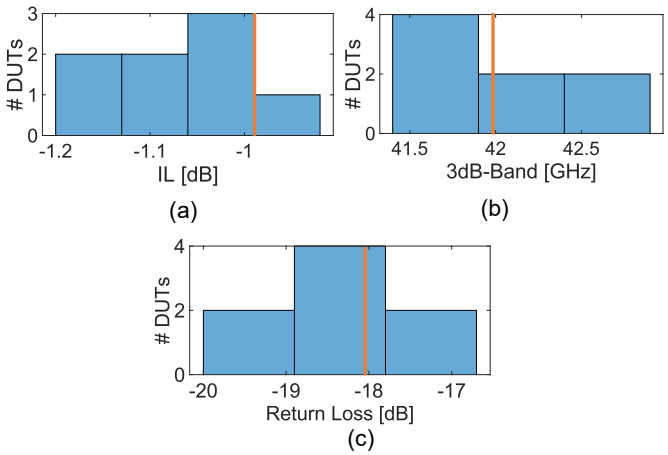

Fig. 9. Distribution of the Insertion Loss (a); 3dB-bandwidth (b); and Return Loss (c) computed for the 8 tuned filters. Orange lines represent the value of the REF device.

convergence. A thermo-electric cooler (TEC) is used to stabilize the temperature of the whole chip. More details about the calibration recipe can be found in [23]. The control loop converged in few tens of milliseconds (< 100 ms) for any of the 8 considered DUTs, a duration that is negligible with respect the I/O optical alignment with the photonic chip. The convergence time corresponds to few tens of iterations, and it is inherently lower bounded by the speed of the thermo-optic actuators (around 10 μs).

The MSE between the spectral response of each DUT filter and the REF filter are reported in Fig. 8(c), for Drop and Through ports (orange curves). Since the MSE for Through response is about one order of magnitude higher than MSE for the Drop response, the minimization of the power at the Through port of the DUT ($P_{O_{PS}}$) provides a more accurate metric for finely tuning the filter compared to the maximization of the Drop port power ($P_{O_{PP}}$). The accuracy of the cloning procedure can be quantified (and DUTs can be classified) by evaluating some relevant metrics of the filter parameters. Figure 9 shows the insertion loss (a), the 3dB-bandwidth (b), and return loss (c) of the 8 filters in their final tuning state. It can be observed that these parameters are very close to the values of the reference filter (orange line), showing a variability lower than 0.12 dB for the insertion loss, 0.60 GHz for the bandwidth and 2 dB for return loss (averaged on 20 GHz around central frequency).

Once the cloning technique reaches convergence and the single DUT can be considered suitable (from both optical and electrical standpoints), its actuators' working points (i.e., voltages, currents or absorbed electrical power) can be stored in LookUp Table (LUT) [23]. In so doing, after testing stage and during normal operation, the state of the PIC can be easily recovered, avoiding the execution of other tuning techniques.

V. Conclusion

We presented and experimentally validated a new approach to perform optical testing of complex photonic integrated filters. In this scenario, testing does not involve merely measurements, but also fast and effective calibration. Instead of tuning the DUT by measuring its spectral response and making it compliant with a specific frequency mask (as in conventional approaches), we use a REF filter to shape the PSD of a broadband source and we measure the optical power collected by a simple photodetector coupled to the output port of the DUT. The strong correlation between the measured optical power and the MSE between the REF and DUT amplitude spectral responses enables us to estimate without ambiguity how far is the DUT from the desired working point and to calibrate the DUT to match desired specifications. With respect to conventional techniques for PIC testing and tuning, our method allows a simple and fast classification and tuning of a DUT with neither estimating the transfer matrix nor measuring the intensity frequency response.

Experimental results on a silicon photonic coupled-MRR filter show good performance both in terms of accuracy in the fine tuning of the spectral response and in the repeatability of the automated procedure, thus leading to a reliable testing routine. Notably, this approach is fast enough (< 100 ms) to be compliant with volume testing requirements.

The method is valid for generic frequency selective devices with arbitrary circuital topologies as well as made in different platforms. It can be applied for PICs with different control variables (not only MRRs phases) implemented with different kind of actuators and power monitors [26]. Furthermore, REF and DUT can be implemented exploiting different technologies and different architectures, not necessarily integrated in the same chip. In case of wafer-level-testing, an external REF can be cascaded to a broadband source and placed before the optical probing station, coupling into the DUT an optical beam with a suitably shaped PSD. Conveniently, the external REF can be a packaged device with its control electronics, that has been previously calibrated and is well stabilized against thermal drifts. This approach could be also employed together with dimensionality reduction and machine learning strategies [27].

Finally, like other testing methods based on intensity monitoring, our approach does not allow testing and tuning of the phase response of the DUT. For all-pole filters (coupled-MRR filter presented in our work), the phase response is uniquely associated to the intensity response (net of a wavelength independent delay), so that the DUT complex response can be recovered with no ambiguity on phase dispersion. Phase observation requires time-consuming interferometric techniques, that are not currently suitable for volume testing and will be the subject of future investigations.

Acknowledgment

The authors acknowledge the staff of Polifab (www.polifab.polimi.it), the microelectronic facility of Politecnico di Milano, for the support in the assembly of photonic chips. The authors also acknowledge R. Baldi for the support in the implementation of the electronic boards. The work has been carried out within the JRC T3 ficonTEC-PoliMi on Techniques and Tooling for Testing in photonics.

References

[1] D. Thomson, A. Zilkie, J. E. Bowers, T. Komljenovic, G. T. Reed, L. Vivien, D. Marris-Morini, E. Cassan, L. Virot, J.-M. Fédéli, J.-M. Hartmann, J. H. Schmid, D.-X. Xu, F. Boeuf, P. O'Brien, G. Z. Mashanovich and M. Nedeljkovic, "Roadmap on silicon photonics," *Journal of Optics,* vol. 18, no. 7, 2016.

[2] M. L. Bushnell and V. D. Agrawal, Essentials of Electronic Testing for Digital, Memory and Mixed-Signal VLSI Circuits, New York, NY: Springer, 2002.

[3] S. Latkowski, D. Pustakhod, M. Chatzimichailidis, W. Yao and X. J. M. Leijtens, "Open Standards for Automation of Testing of Photonic Integrated Circuits," *Journal of Selected Topics on Quantum Electronics,* vol. 25, no. 5, pp. 1-8, 2019.

[4] A. Rahim, T. Spuesens, R. Baets and W. Bogaerts, "Open-Access Silicon Photonics: Current Status and Emerging Initiatives," *Proceedings of the IEEE,* vol. 106, no. 12, pp. 2313-2330, 2018.

[5] Y. Wang, P. Sun, J. Hulme, S. A. M., M. Fiorentino, R. G. Beausoleil and K.-T. Cheng, "Energy Efficiency and Yield Optimization for Optical Interconnects via Transceiver Grouping," *Journal of Lightwave Technology,* vol. 39, no. 6, pp. 1567-1578, 2021.

[6] Z. Lu, J. Jhoja, J. Klein, X. Wang, A. Liu, J. Flueckiger, J. Pond and L. Chrostowski, "Performance prediction for silicon photonics integrated circuits with layout-dependent correlated manufacturing variability," *Optics Express,* vol. 25, pp. 9712-9733, 2017.

[7] P. Sun, J. Hulme, T. Van Vaerenbergh, J. Rhim, C. Baudot, F. Boeuf, N. Vulliet, A. Seyedi, M. Fiorentino and R. G. Beausoleil, "Statistical Behavioral Models of Silicon Ring Resonators at a Commercial CMOS Foundry," *IEEE Journal of Selected Topics in Quantum Electronics,* vol. 26, no. 2, pp. 1-10, 2020.

[8] C. Cui and Z. Zhang, "Stochastic Collocation With Non-Gaussian Correlated Process Variations: Theory, Algorithms, and Applications," *IEEE Transactions on Components, Packaging and Manufacturing Technology,* vol. 9, no. 7, p. 2019, 2018.

[9] F. Morichetti, S. Grillanda and A. Melloni, "Breakthroughs in Photonics 2013: Toward Feedback-Controlled Integrated Photonics," *IEEE Photonics Journal,* vol. 6, no. 2, 2014.

[10] H. Jayatilleka, K. Murray, M. A. Guillen-Torres, M. Caverley, R. Hu, N. A. F. Jaeger, L. Chrostowsky and S. Shekhar, "Wavelength tuning and stabilization of microring-based filters using silicon in-resonator photoconductive heaters," *Optics Express,* vol. 23, no. 19, pp. 25084-25097, 2015.

[11] P. Dumais, D. J. Goodwill, D. Celo, J. Jiang, C. Zhang, F. Zhao, X. Tu, C. Zhang, S. Yan, J. He, M. Li, W. Liu, Y. Wei, D. Geng, H. Mehrvar and E. Bernier, "Silicon Photonic Switch Subsystem With 900 Monolithically Integrated Calibration Photodiodes and 64-Fiber Package," *Journal of Lightwave Technology,* vol. 36, no. 2, pp. 233-238, 2018.

[12] H. Jayatilleka, H. Shoman, L. Chrostowski and S. Shekhar, "Photoconductive heaters enable control of large-scale silicon photonic ring resonator circuits," *Optica,* vol. 6, no. 1, pp. 84-91, 2019.

[13] A. Annoni, E. Guglielmi, M. Carminati, G. Ferrari, M. Sampietro, D. A. B. Miller, A. Melloni and F. Morichetti, "Unscrambling light—automatically undoing strong mixing between modes," *Light: Science and Applications,* vol. 6, 2017.

[14] N. C. Harris, Y. Ma, J. Mower, T. Baehr-Jones, D. Englund, M. Hochberg and C. Galland, "Efficient, compact and low loss thermo-optic phase shifter in silicon," *Optics Express,* vol. 22, no. 9, pp. 10487-10493, 2014.

[15] Q. Xu, S. Manipatruni, B. Schmidt, J. Shakya and M. Lipson, "12.5 Gbit/s carrier-injection-based silicon micro-ring silicon modulators," *Optics Express,* vol. 15, no. 2, pp. 430-436, 2007.

[16] Y. Li and A. W. Poon, "Active resonance wavelength stabilization for silicon microring resonators with an in-resonator defect-state-absorption-based photodetector," *Optics Express,* vol. 23, no. 1, pp. 360-372, 2015.

[17] J. A. Cox, A. L. Lentine, D. C. Trotter and A. L. Starbuck, "Control of integrated micro-resonator wavelength via balanced homodyne locking," *Optics Express,* vol. 22, no. 9, pp. 11279-11289, 2014.

[18] K. Padmaraju, D. F. Logan, T. Shiraishi, J. J. Ackert, A. P. Knights and K. Bergman, "Wavelength Locking and Thermally Stabilizing Microring Resonators Using Dithering Signals," *Journal of Lightwave Technology,* vol. 32, no. 3, pp. 505-512, 2014.

[19] J. C. C. Mak and J. K. S. Poon, "Multivariable Tuning Control of Photonic Integrated Circuits," *Journal of Lightwave Technology,* vol. 35, no. 9, pp. 1531-1541, 2017.

[20] P. Orlandi, F. Morichetti, M. J. Strain, M. Sorel, P. Bassi and A. Melloni, "Photonic Integrated Filter With Widely Tunable Bandwidth," *Journal of Lightwave Technology,* vol. 32, no. 5, pp. 897-907, 2014.

[21] Available in the PDK of AMF, Advanced Micro Foundry, http://www.advmf.com, Singapore, 2022.

[22] F. Morichetti, M. Milanizadeh, M. Petrini, F. Zanetto, G. Ferrari, D. Aguiar, E. Guglielmi, M. Sampietro and A. Melloni, "Polarization-transparent silicon photonic add-drop multiplexer with wideband hitless tuneability," *Nature Communications,* vol. 12, no. 4324, 2021.

[23] M. Milanizadeh, S. Ahmadi, M. Petrini, D. Aguiar, R. Mazzanti, F. Zanetto, E. Guglielmi, M. Sampietro, F. Morichetti and A. Melloni, "Control and Calibration Recipes for Photonic Integrated Circuits," *Journal of Selected Topics in Quantum Electronics,* vol. 26, no. 5, pp. 1-10, 2020.

[24] F. Zanetto, V. Grimaldi, F. Toso, E. Guglielmi, M. Milanizadeh, D. Aguiar, M. Moralis-Pegios, S. Pitris, T. Alexoudi, F. Morichetti, A. Melloni, G. Ferrari and M. Sampietro, "Dithering-based real-time control of cascaded silicon photonic devices by means of non-invasive detectors," *IET Optoelectronics,* vol. 15, pp. 111-120, 2020.

[25] M. Milanizadeh, D. Aguiar, A. Melloni and F. Morichetti, "Canceling Thermal Cross-Talk Effects in Photonic Integrated Circuits," *Journal of Lightwave Technology,* vol. 37, no. 4, pp. 1325-1332, 2019.

[26] A. Perino, F. Zanetto, M. Petrini, F. Toso, F. Morichetti, A. Melloni, G. Ferrari and M. Sampietro, "High-sensitivity transparent photoconductors in voltage-controlled silicon waveguides," *Optics Letters,* vol. 47, no. 6, pp. 1327-1330, 2022.

[27] W. Gao, L. Lu, L. Zhou and J. Chen, "Automatic calibration of silicon ring-based optical switch powered by machine learning," *Optics Express,* vol. 28, no. 7, pp. 10438-10455, 2020.